




Original Research

Fabrication of sulphonated poly(ethylene glycol)-diacrylate hydrogel as a bone grafting scaffold

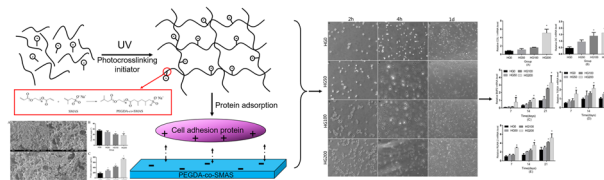
Hao Li¹ · Tingting Ma¹ · Man Zhang¹ · Jiani Zhu¹ · Jie Liu¹ · Fei Tan¹ 

Received: 14 June 2018 / Accepted: 27 November 2018 / Published online: 7 December 2018
© Springer Science+Business Media, LLC, part of Springer Nature 2018

Abstract

To improve the biological performance of poly(ethylene glycol)-diacrylate (PEGDA) hydrogel as an injectable bone grafting scaffold, sodium methallyl sulphonate (SMAS) was incorporated into PEGDA hydrogel. The physicochemical properties of the resultant polymers were assessed via Fourier transform infrared spectroscopy (FTIR), swelling ratio, zeta potential, surface morphology, and protein adsorption analysis. MC3T3-E1 cells were seeded on the hydrogel to evaluate the effect of the sulphonated modification on their attachment, proliferation, and differentiation. The results of FTIR and zeta potential evaluations revealed that SMAS was successfully incorporated into PEGDA. With increasing concentrations of SMAS, the swelling ratio of the hydrogels increased in deionized water but stayed constant in phosphate buffered saline. The protein adsorption also increased with increasing concentration of SMAS. Moreover, the sulphonated modification of PEGDA hydrogel not only enhanced the attachment and proliferation of osteoblast-like MC3T3-E1 cells but also up-regulated alkaline phosphatase activity as well as gene expression of osteogenic markers and related growth factors, including collagen type I, osteocalcin, runt related transcription factor 2, bone morphogenetic protein 2, and transforming growth factor beta 1. These findings indicate that the sulphonated modification could significantly improve the biological performance of PEGDA hydrogel. Thus, the sulphonated PEGDA is a promising scaffold candidate for bone grafting.

Graphical Abstract



1 Introduction

Defects in the alveolar bone can interfere with the dental prosthetic rehabilitation, particularly those being restored with dental implant therapy. In clinic, current strategies often involve various alveolar bone grafting procedures, but both autogenous and heterogeneous cancellous grafts are neither practical nor expedient. Meanwhile, the characteristics of alveolar bone defects, such as large size, complicated shape and deep location, make it difficult to be perfect restored. The development of injectable hydrogels affords a new method to restoring alveolar bone defects, because hydrogels can replace implantation surgery with a minimally invasive injection method and can form any desired shape to match irregular defects.

These authors contributed equally: Hao Li and Tingting Ma

✉ Fei Tan
tanf-1984@163.com
Jie Liu
18661801995@163.com

¹ Department of Prosthodontics, the Affiliated Hospital of Qingdao University, Qingdao University, 266003 Qingdao, People's Republic of China

Photopolymerizable poly(ethylene glycol)-diacrylate (PEGDA) is an important synthetic hydrogel for biomedical applications such as drug delivery, regenerative medicine, and the development of biosensors [1–3]. PEGDA is a promising bone grafting scaffold candidate because of its biocompatibility, tuneable mechanical properties, three-dimensional porous structure, ability to homogeneously encapsulate cells, and high tissue-like water content. Comparing with the natural hydrogels, the synthetic hydrogels, such as PEGDA, still have some advantages. In addition to non-immunogenicity, the PEGDA is relative ease of functionalization with biomolecular motifs and/or small functional groups [4]. Meanwhile, as with other synthetic hydrogels, PEGDA show better commercial availability of reactive macromers of various molecular weights and branching configurations, which might be a limitation for natural hydrogels. However, the hydrated surface layer formed on the PEGDA surface inhibits the adsorption of specific adhesion proteins, such as fibronectin (Fn), resulting in a lower cell attachment rate on the hydrogel [5, 6]. This limits PEGDA bone grafting scaffold applications.

Cell attachment onto the scaffold plays a decisive role in regulating cell proliferation and promoting osteoblastic differentiation. Various modifications have been applied to improve cell attachment onto PEGDA. For example, arginine-glycine-aspartic (RGDS) immobilization into PEGDA could promote cell attachment on the hydrogel [7]. However, the process of bone development is inherently dependent on the interaction between osteoblasts and extracellular matrix (ECM) proteins. It has been well established that the major adhesion proteins in bone, such as Fn, function through mechanisms other than RGDS-integrin binding [8, 9]. For example, a heparin-binding domain in Fn of bone-derived cells has been found to play an important role in osteoblastic attachment [10]. Moreover, ECM is still difficult to deposit on the PEGDA modified with RGD [4]. Another approach to improve the cell attachment to hydrogels is to change the physicochemical properties of the material surface. It has been demonstrated repeatedly that osteoblastic attachment to an artificial hydrogel depended strongly on the physicochemical properties of the material surface, such as its chemical composition, polarity, and charge density [11–13].

The chemical functionality of an artificial hydrogel has a direct influence on the differentiation fate of attached cells. For example, it was proven that hydrogel-encapsulated human mesenchymal stem cells could be induced to osteogenesis by the hydrogel modified with different functional molecular [4, 14]. On the one hand, it was found that the sulphonated polystyrene surface could convert Fn from a soluble dimer to insoluble stable matrix fibrils by inducing disulphide bond rearrangement [10, 15, 16]. On the other

hand, the charge could improve the protein adsorption onto the hydrogel surface [13]. The charged group might promote cell attachment by improving protein adsorption and unfolding protein conformation [17]. In our previous study, we found that a charged hydrogel would be helpful to improve the pre-osteoblastic attachment, proliferation, and differentiation regardless of positive or negative charge [11]. However, until now, few studies have demonstrated the effects of the incorporation of a charged sulphonated group into PEGDA hydrogel on the attachment, proliferation, and differentiation of osteoblasts.

In this study, sodium methallyl sulphonate (SMAS), a small molecule monomer with a charged sulphonated group, was incorporated into PEGDA to produce a novel hydrogel for use as a bone grafting scaffold. We hypothesized that this novel hydrogel can enhance the attachment, proliferation, and differentiation of osteoblasts. Therefore, various concentrations of SMAS were incorporated into PEGDA, and the physicochemical properties of the resultant polymers were evaluated. In addition, pre-osteoblasts were seeded on the hydrogels to evaluate the effect of the charged sulphonated group on the cell viability, proliferation, and differentiation *in vitro*.

2 Materials and methods

2.1 Preparation of PEGDA

PEGDA was synthesized as described in our previous study [11]. Dry PEG (0.1 mM; $M_w = 4000$ Da; Sino-pharm Co. Ltd, Shanghai, China) and 0.2 mM triethylamine were dissolved in anhydrous dichloromethane at room temperature. Then, 0.4 mM acryloyl chloride was added dropwise in an ice bath and stirred for 24 h. The resultant solution was washed with 2 M K_2CO_3 aqueous solution and separated into aqueous and dichloromethane phases. The dichloromethane phase was subsequently dried with anhydrous $MgSO_4$, and PEGDA was precipitated in diethyl ether, filtered by filter paper, and dried under a vacuum.

2.2 Hydrogel preparation

PEGDA aqueous solution was prepared at a final concentration of 40% by dissolving 2 g PEGDA powder in 5 mL HEPES solution. Photoinitiator D2959 (0.1 g; Sigma-Aldrich, St. Louis, MO, USA) was dissolved in 20 mL HEPES solution to obtain a final concentration of 0.5% D2959 solution. It was then filtered and preserved avoiding light. SMAS (0.633 g; Sigma-Aldrich, St. Louis, MO, USA) was dissolved in 2 mL HEPES solution to obtain 2 M SMAS aqueous solution. All solutions were magnetically

Table 1 Preparation of hydrogels modified with different concentrations of SMAS

Group	PEGDA (mL)	D2959 (μL)	SMAS (μL)	HEPES (μL)	Volume (mL)
HG0	1	400	0	600	2
HG50	1	400	50	550	2
HG100	1	400	100	500	2
HG200	1	400	200	400	2

stirred for 30 min to ensure that the materials were completely dissolved.

As shown in Table 1, the hydrogel precursors containing 0, 50, 100, and 200 mM SMAS were prepared, respectively (abbreviated as HG0, HG50, HG100, and HG200). The PEGDA/SMAS mixture was pipetted onto two sterile glass slides. There was a 1 mm spacer between the glass slides. Then, the area was irradiated for 15 min using ultraviolet light (365 nm, 8 mW cm⁻²).

2.3 Fourier-transform infrared spectroscopy

After lyophilization for 24 h, the chemical structures of the hydrogels were characterized using a Fourier-transform infrared (FTIR; NICOLET380, USA) spectrophotometer ($N = 3$).

2.4 Zeta potential

The hydrogel samples in each group ($N = 6$) were immersed in deionized water to achieve the equilibrium state and ground into fine particles. After drying in a vacuum oven, 5 mg of the particles were dissolved in 1 mL deionized water and the zeta potential was measured by a Zetasizer instrument (Zen3600, Malvern Instruments, Malvern, UK).

2.5 Swelling ratio

To obtain equilibrium swelling, hydrogel samples ($N = 6$) were immersed in deionized water or phosphate buffered saline (PBS) for 24 h at 37 °C, respectively. Then, excess water was removed with filter paper, and the swollen hydrogels were weighed (W_s , swollen weight). The samples were put in a vacuum oven at 50 °C for 24 h to achieve complete dehydration and to determine the dry weight of the samples (W_d , final dry weight). The swelling ratio was calculated as follows: Swelling ratio = $(W_s - W_d)/W_d$.

2.6 Contact angle measurement

Hydrogels from each group ($N = 6$) were swollen in PBS until reaching the equilibrium state. Then, the static water contact angle of the hydrogels was observed using the

sessile drop method at room temperature by a contact angle goniometer (SL200B, KINO INDUSTRY Co., Ltd., USA). The contact angle was recorded digitally using the software provided by the manufacturer.

2.7 Elastic modulus

Uniaxial compressive test was performed to evaluate the elastic modulus of the unmodified hydrogel and PEGDA-co-SMAS hydrogels. The hydrogels (8 mm in diameter, 2 mm in thickness, $N = 4$) of each group were crosslinked. Then, the load cell was placed at the bottom plate of an electromechanical universal testing machine (Shimadzu AGS-J, Tokyo, Japan). Meanwhile, a digital cross-head sensor was placed to the top plate at a strain rate of 0.5 mm/min. The stress–strain curve was recorded digitally using the software provided by the manufacturer. Compressive modulus was calculated from the slope of the initial 5% linear region of the respective stress–strain curves.

2.8 Protein adsorption

Hydrogels from each group ($N = 5$) were placed into 12-well plates and immersed in Alpha modified Eagle's medium (α -MEM, Hyclone, Logan, USA) supplemented with 10% foetal bovine serum (FBS; Hyclone, Logan, USA) at 37 °C for 24 h. Then, the samples were moved to new plates after washing three times with PBS. One millilitre of 1% sodium dodecyl sulphate (SDS; Sigma-Aldrich, St. Louis, MO, USA) solution was added into each well and stirred for 24 h to completely remove absorbed proteins from the hydrogel. The protein concentrations of the SDS solutions were determined by BCA Protein Assay Reagent (Beyotime, Guangzhou, China).

2.9 Scanning electron microscopy observation

After freeze-drying under a vacuum, the hydrogels from each group were sputter-coated with gold-palladium. Scanning electron microscopy (SEM, Hitachi S-4800, Tokyo, Japan) was used to observe the morphology of the hydrogels.

2.10 Cell culture

Mouse calvaria-derived pre-osteoblast, MC3T3-E1 cells, were purchased from American Type Culture Collection (ATCC) and cultured in α -MEM supplemented with 10% foetal bovine serum (FBS), 100 U/ml penicillin, and 100 U/ml streptomycin in a 37 °C, 5% CO₂ incubator. The cells were subcultured to approximately 80% confluency. The cell culture medium was replaced every 1–2 days.

2.11 Cell attachment

The hydrogel samples ($N=6$) were placed into 24-well plates, and the cells were seeded on the hydrogel surface at a density of 1×10^4 cells/cm². Then, the cells were allowed to attach for 2 h, and subsequently supplemented with 3 mL medium. At specific time points, the hydrogels were transferred to new 6-well plates, rinsed twice with PBS to remove the unattached cells. After 2 h, 4 h, and 1 day, the cells were observed by phase-contrast microscopy (CP62-JSM-6390LV, Beijing, China).

2.12 Cell proliferation

A Cell Counting Kit-8 assay (CCK-8; Beyotime Institute of Biotechnology, Guangzhou, China) was used to evaluate the osteoblastic proliferation on the hydrogels. At days 1, 3, and 5, CCK-8 assays were performed to determine the cell viability according to the manufacturer's instructions. In brief, after changing the medium, 20 μ L CCK-8 solution was added into 200 μ L of cell/hydrogel medium. Then, the medium was transferred to 96-well plates and optical density (OD) values were determined at 450 nm using a micro-plate reader (Synergy H1, BioTek Instruments, USA) after incubation at 37 °C for 3 h.

2.13 Alkaline phosphatase (ALP) activity

To detect ALP activity, p-nitrophenyl phosphate liquid substrate (pNPP) was mixed with the supernatant of the cell lysate. Briefly, MC3T3-E1 cells were seeded onto each hydrogel sample at a density of 4×10^5 cells/mL and cultured in 1.5 mL medium supplemented with 0.2 mM ascorbic acid (Sigma-Aldrich, St. Louis, MO, USA). At 7, 10, and 14 days, each specimen was lysed in 0.2% Triton X-100 for 4 h and centrifuged at 12,000 rpm for 15 min at 4 °C. Then, 15 μ L supernatant was added into 2-amino-2-methyl-1-propanol (AMP) buffer solution containing 15 mmol/L pNPP and incubated at 37 °C for 30 min. After that, 0.1 M sodium hydroxide solution was used to terminate the reaction, and the absorbance was recorded at 405 nm using a micro-plate reader. Meanwhile, the total protein content in the supernatant was calculated with the BCA Protein Assay Reagent. The ALP activity was normalized to the total protein concentration.

2.14 Quantitative real-time polymerase chain reaction (RT-PCR)

To evaluate the gene expression of osteogenic markers and related growth factors, total RNA was extracted via Trizol (Aidlab, Beijing, China) after 7, 14, and 21 days. The RNA concentration was determined by absorbance measurement

at 280 nm. One microgram of total RNA was reverse-transcribed for cDNA using the ReverTra Ace reaction system (TaKaRa Bio, Shiga, Japan). Quantitative real-time polymerase chain reaction (RT-PCR) was performed to evaluate the related gene expression level. All samples were tested in triplicate. The primers used are shown in Table 2.

2.15 Statistical analysis

All data were analysed as the mean \pm standard deviation (SD). One-way analysis of variance (ANOVA) was performed using SPSS (SPSS19.0; SPSS Inc., USA) to determine the statistical significance among the groups. Statistical significance was defined as $P < 0.05$.

3 Results

3.1 FTIR spectra

The chemical structure of PEGDA and the reaction of PEGDA with SMAS are shown in Fig. 1. According to the results of FTIR, a new peak was found at 1105 cm⁻¹ and was ascribed to the carboxylic acid groups of SMAS (Fig. 2). Meanwhile, the intensity of the peak strengthened with the increasing concentration of SMAS.

3.2 Swelling ratio and zeta potential

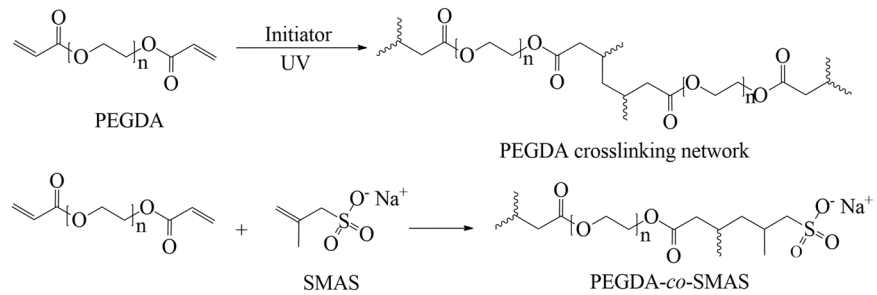
Table 3 shows the swelling ratio of hydrogels copolymerized with different concentrations of SMAS in deionized water or PBS, respectively. The results indicated that the swelling ratio of the hydrogels significantly increased with increasing concentration of SMAS in deionized water ($P < 0.05$). However, the sulphonated modification of the PEGDA hydrogel had almost no effect on the swelling ratio in PBS ($P > 0.05$). We found that the zeta potentials of hydrogels modified with SMAS became more negative (Table 3). Meanwhile, the charge density of PEGDA-co-SMAS increased with the increasing SMAS concentration. All of the PEGDA-co-SMAS hydrogels were more negative than HG-0 ($P < 0.05$). For example, the zeta potential of HG0 was initially 1.01 ± 0.13 mV, and it reached -3.82 ± 0.25 when 200 mM SMAS was incorporated into the PEGDA hydrogel.

3.3 SEM observation, contact angle measurement and protein adsorption

The hydrogels were observed by SEM to evaluate the effect of sulphonate modification on the surface morphology of the PEGDA hydrogel. As shown in Fig. 3A, all of the hydrogels exhibited a three-dimensional interconnected

Table 2 Primers sequences for RT-PCR

Gene	Forward primer	Reverse primer
TGFβ1	AGCTGCGCTTGCAGAGTTA	AGCCCTGTATTCCGTGTGGT
BMP-2	GAGGCTGCTCAGCATGTTTG	CTCCACGGCTTCTTCGTGAT
Runx-2	GGGAACCAAGAAGGCACAGC	ACTTGGTGCAGAGTTCAGGG
COL 1	GAGAGGTGAACAAGGTCCCC	AAACCTCTCTCGCCTCTTGC
OC	TTCTGCTCACTCTGCTGACC	GCCGGAGTCTGTTCCTACTACC

Fig. 1 Chemical structure of PEGDA and the reaction of PEGDA with SMAS**Table 3** Swelling ratio and zeta potential of hydrogels incorporated with different concentrations of SMAS ($x \pm s$)

Groups	Swelling ratio(%)		Zeta potential (mV)
	ddH ₂ O	PBS	
HG0	19.45 ± 0.52	27.50 ± 0.72	1.01 ± 0.13
HG50	29.76 ± 2.15*	28.85 ± 3.89	-1.64 ± 0.24*
HG100	34.45 ± 3.47*	29.10 ± 2.82	-2.59 ± 0.28*
HG200	48.01 ± 3.81*	29.43 ± 3.28	-3.82 ± 0.25*

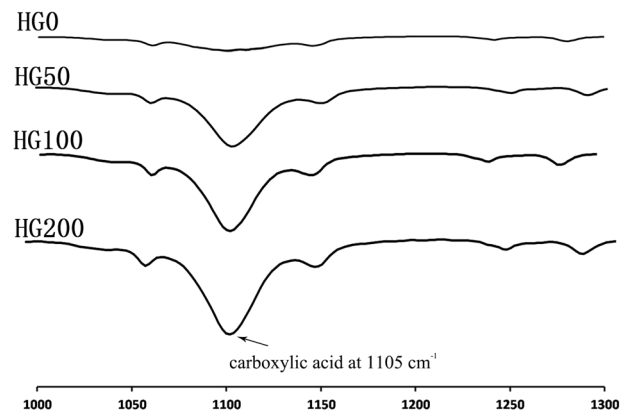
The data were presented as the mean ± SD

*indicates significant differences, compared with HG-0 ($P < 0.05$)

porous structure regardless of the concentration of SMAS. However, the sulphonate modification influenced the pore sizes in the hydrogels. For example, the pore sizes in the HG0 group were relatively homogeneous and ranged from 5 to 10 μm (Fig. 3Aa). However, in contrast with HG0, the pore sizes of the HG200 group were more irregular and ranged from 5 to 50 μm .

Contact angles of the hydrogels copolymerized with various concentrations of SMAS are shown in Fig. 3B. The surface contact angle decreased with increasing concentration of SMAS, which indicated an enhanced hydrophilicity of the hydrogels surface. However, no significant difference was found between the HG50 and HG0 group ($P > 0.05$).

The protein adsorptions of the four hydrogels are shown in Fig. 3C. It was found that the amount of absorbed protein increased in a dose-dependent manner with the increasing concentrations of SMAS in the hydrogel precursor. For example, compared with HG0, HG100 and HG200 showed 2.3-fold and 3.9-fold increases in the amount of absorbed protein, respectively. These results clearly demonstrated

**Fig. 2** The FTIR spectra of hydrogels modified with different concentrations of SMAS

that the incorporation of the sulphonated group could effectively enhance the protein adsorption of the hydrogel.

3.4 Elastic modulus

The elastic modulus of samples in each group was shown in Fig. 4. We found that the elastic modulus remained constant even if the concentration of the SMAS monomers incorporated into the PEGDA backbone increased. For example, the elastic moduli were 8.82 ± 0.43 kPa for HG0 and 8.86 ± 0.62 kPa for HGP200. The difference was not statistically significant ($P > 0.05$).

3.5 Cell attachment

The morphologies of the attached cells on the four hydrogels are shown in Fig. 5. After 2 h culture, almost all the

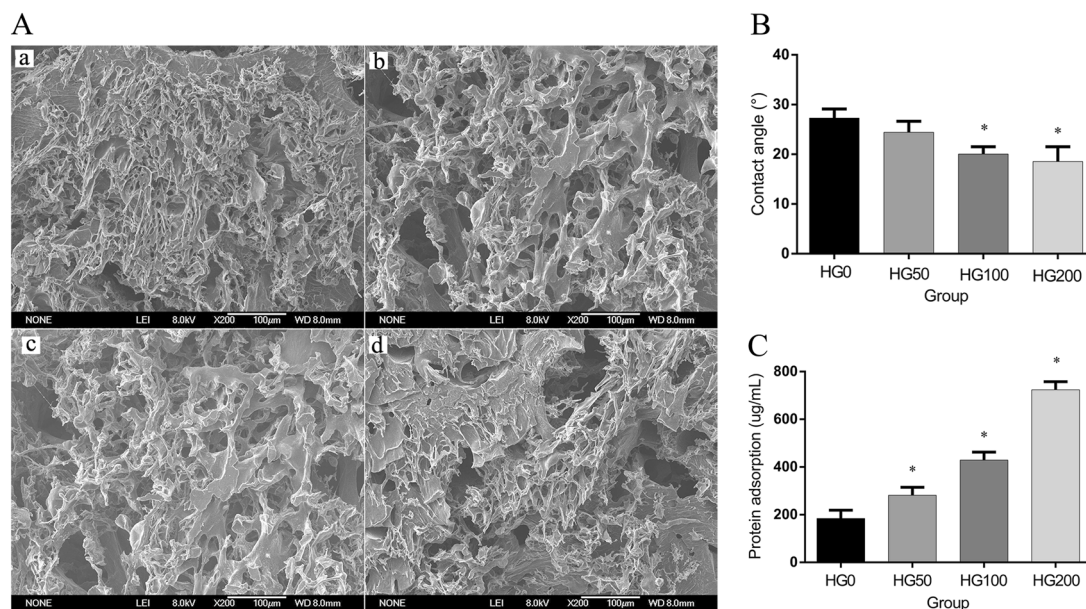


Fig. 3 Physicochemical properties of the hydrogels modified with different concentrations of SMAS. **A** surface morphology of the hydrogels: **a** group HG0; **b** group HG50; **c** group HG100; **d** group HG200.

B contact angle of the hydrogels ($N=6$). **C** protein adsorption of the hydrogels ($N=5$). *indicates significant differences, compared with HG-0 ($P<0.05$)

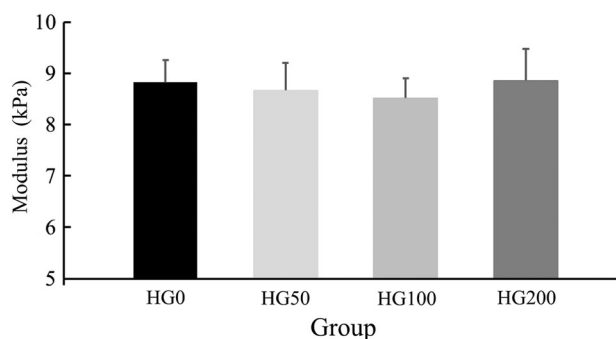


Fig. 4 The elastic modulus of different hydrogels ($N=4$)

cells on the surface of HG0 maintained a spherical shape. However, many cells on the PEGDA-co-SMAS hydrogel started to spread and presented short pseudopodia. At 4 h, almost all the cells on the surface of the PEGDA-co-SMAS had demonstrated fusiform or polygonal shapes. Additionally, all the cells formed solid adhesion on both unmodified hydrogels and PEGDA-co-SMAS after 1-day incubation. However, more cells were found on the sulphonated hydrogels compared with HG0.

3.6 Cell proliferation

CCK-8 was used to assess the effect of sulphonate modification on the osteoblastic proliferation. As shown in Fig. 6, MC3T3-E1 cells on both PEGDA hydrogels and modified hydrogels proliferated over time, but there were significantly more cells on the HG100 and HG200 surfaces than there were on the HG-0 surface at each time point ($P<$

0.05), including 1 day, 3 days, and 5 days. However, there was no difference between the HG-0 and HG-50 groups ($P>0.05$).

3.7 Alkaline phosphatase (ALP) activity

The ALP activity of the cells cultured on all hydrogels is shown in Fig. 7. As shown, in contrast with the HG0 group, the ALP activity of the HG100 and HG200 groups was significantly improved at each time point ($P<0.05$), including 7 days, 10 days, and 14 days. For example, after 14 days of induction, the ALP activity of cells cultured on HG100 and HG200 increased by about 0.40-fold and 0.50-fold that of HG0, respectively. Nevertheless, there was no significant difference between the HG0 and HG50 group ($P>0.05$) over the whole experimental period.

3.8 RT-PCR

To further evaluate the effect of sulphonate modification on the osteoblastic differentiation, the gene expression levels of osteogenic markers and related growth factors were investigated by RT-PCR (Fig. 8). The results revealed that, compared with the HG0 group, enhanced gene expression of osteogenic markers and growth factors was found in the HG200 group ($P<0.05$). For instance, after 21 days incubation, the OC gene expression of HG200 increased 2.57-fold compared with that of the HG0 group. In contrast with the HG0 group, the osteogenic gene expression in the HG100 group was enhanced with increasing culture time.

Fig. 5 Morphology of adherent cells on the hydrogels modified with different concentrations of SMAS **a** cell morphology on HG0 group at 2 h, **b** cell morphology on HG0group at 4 h, **c** cell morphology on HG0group at 1 day, **d** cell morphology on HG50group at 2 h, **e** cell morphology on HG50group at 4 h, **f** cell morphology on HG50group at 1 day, **g** cell morphology on HG100group at 2 h, **h** cell morphology on HG100group at 4 h, **i** cell morphology on HG100group at 1 day, **j** cell morphology on HG200group at 2 h, **k** cell morphology on HG200group at 4 h, **l** cell morphology on HG200 group at 1 day

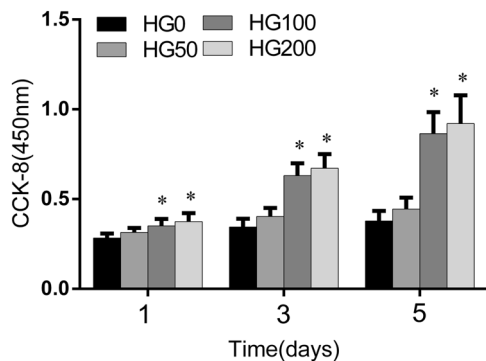
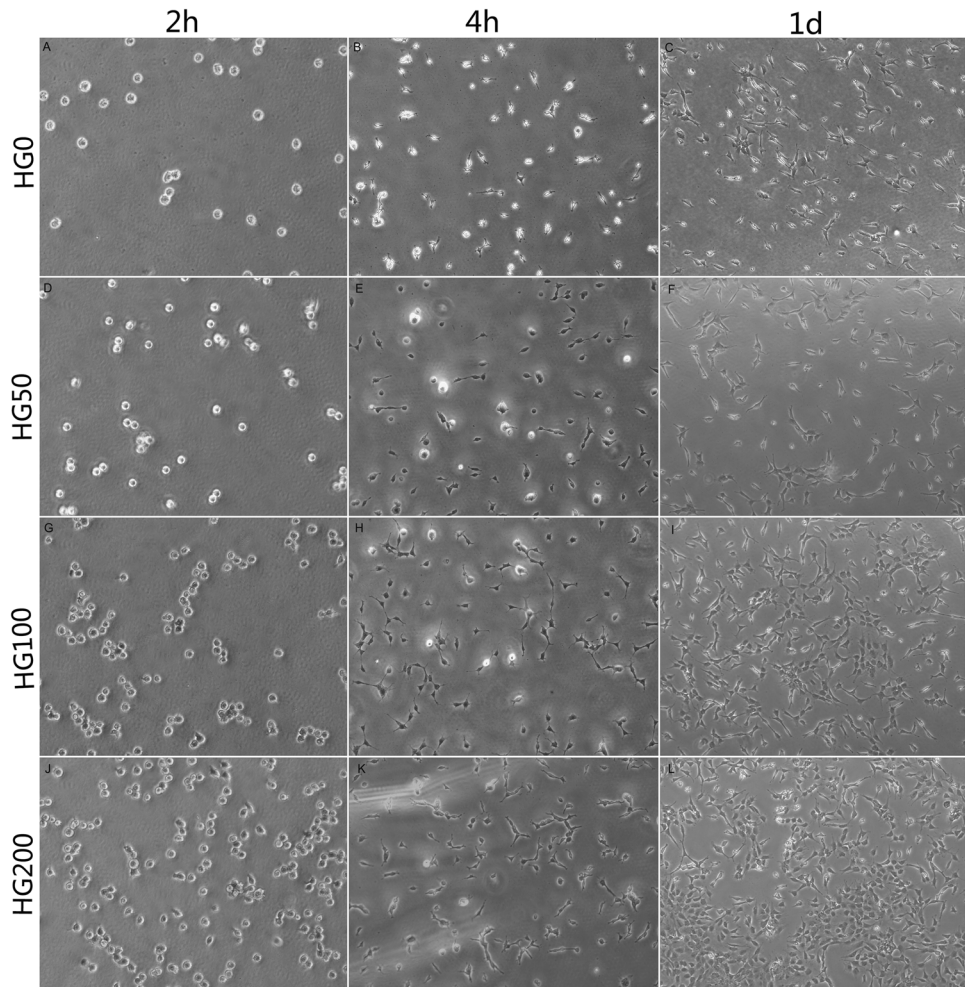


Fig. 6 Cell proliferation of MC3T3-E1 cell cultured with four hydrogels at days 1,3,5. *indicates significant differences, compared with HG-0($P < 0.05$)

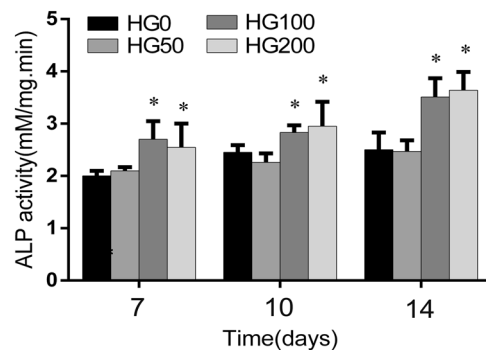


Fig. 7 ALP activity of cells cultured on the four hydrogels. *indicates significant differences,compared with HG-0 ($P < 0.05$)

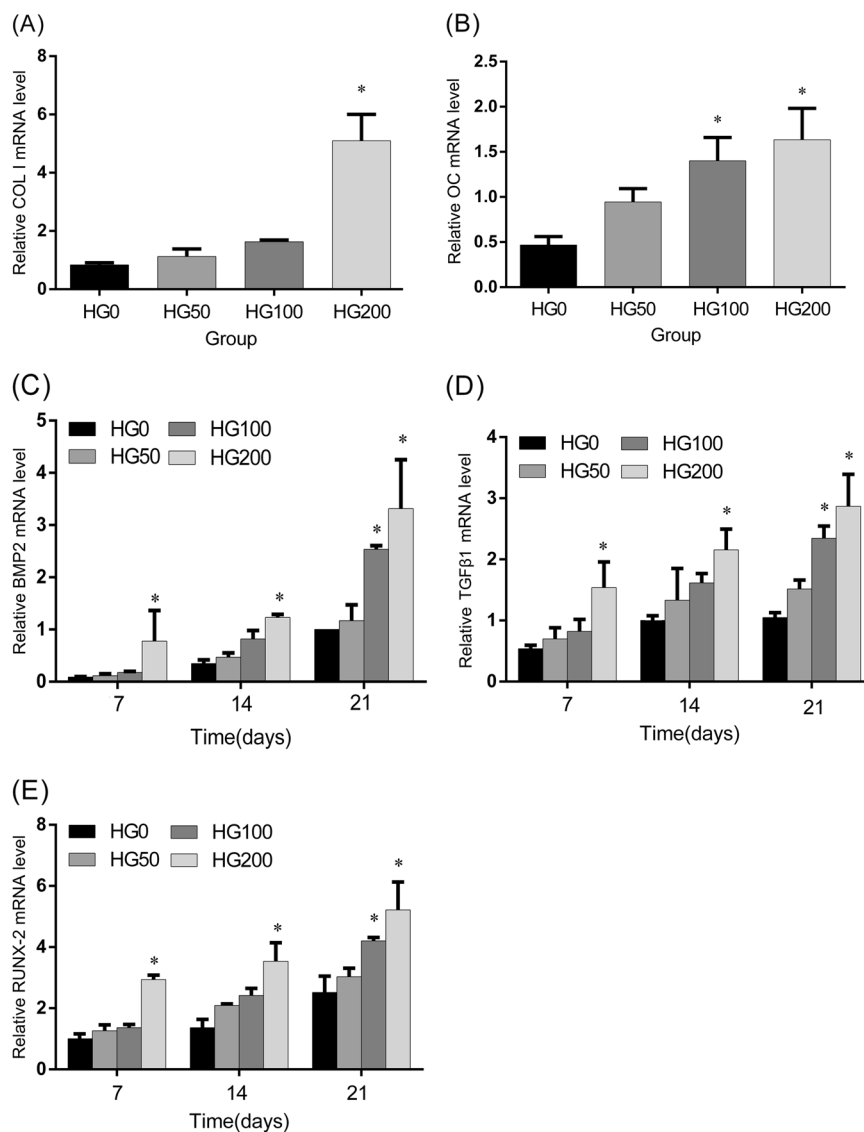
For example, although there was no significant difference in BMP2 gene expression between HG0 and HG100 groups at 14 days, the BMP2 gene expression of the HG100 group increased 2.13-fold at 21 days. Similar tendencies were found in the gene expression levels of both osteogenic markers and related growth factors. However, there was no

significant difference between HG0 and HG50 groups over the cultivation period ($P > 0.05$).

4 Discussion

An important goal of bone grafting scaffold is to create a structure that mimics native bone biochemically and

Fig. 8 Expression of osteogenic marker genes and related growth factors for cells cultured on the hydrogels ($N=6$). **a** COLI, **b** OC, **c** BMP2, **d** TGF β 1, **e** RUNX-2. *indicates significant differences, compared with HG-0 ($P < 0.05$)



structurally [18]. The ideal scaffold should not only mimic critical aspects of the natural osteoblastic micro-environment but also promote osteoblastic differentiation through cell-material interactions [19, 20]. Studies have repeatedly demonstrated that a small functional group can be used to control the biological behaviour of hydrogel-encapsulated cells [16, 21, 22]. In this study, the sulphonate group was introduced into the hydrogel by copolymerization of PEGDA with various concentrations of SMAS. The results clearly indicated that the sulphonated PEGDA hydrogels had physicochemical properties that could be varied in a controllable manner. Moreover, the hydrogels significantly enhanced the attachment, proliferation, and differentiation of osteoblast-like cells.

According to FTIR, SMAS was successfully incorporated into the PEGDA hydrogel, and the modification was dose-dependent. Meanwhile, the successful incorporation

was indirectly verified by the zeta potential measurement in which the zeta potential increased with increasing SMAS concentration in the hydrogel precursor. In theory, the zeta potential of hydrogels should stem from the deprotonation of hydroxy group in the SMAS. On the one hand, this result indicated that the SMAS was incorporated into the PEGDA hydrogel in a dose-dependent manner; on the other hand, the charge density of the modified hydrogel could increase with the increasing concentration of SMAS in the hydrogel precursor [23, 24]. The swelling ratio increased in deionized water with the increasing concentration of SMAS. In theory, this should be attributed to the competitive incorporation of SMAS onto the unsaturated bond of the acrylate group in PEGDA. Since the unsaturated bonds serve as the cross-linking site for PEGDA macromolecules as well, the modification would decrease the availability of unsaturated bonds and lead to a loose polymeric cross-linked network in

modified hydrogels. The hypothesis could be verified by the morphology observation. As shown in Fig. 3A, all hydrogels presented a three-dimensional interconnected fibril network. In the case of modified hydrogels, the network was more porous than that of the HG0 group, and the pore size was $\sim 50\ \mu\text{m}$. It has been demonstrated that a loose polymeric network in a hydrogel could facilitate nutrient transport, metabolic waste discharge, and cell migration [25, 26]. However, an increase in the swelling ratio was not observed in scaffolds submerged in PBS. This result may be associated with a balance of osmotic pressure between the charged hydrogel and PBS. Because of the effect of electrostatic attraction on the modified hydrogel, counterions are more easily adsorbed onto the modified hydrogel, and the modified hydrogel could quickly achieve a balance between internal and external osmotic pressure.

The attachment and proliferation of MC3T3-E1 cells were enhanced on the modified hydrogels, and the enhancement was closely related to the concentration of SMAS in the hydrogel. It has been repeatedly reported that a low cell attachment and proliferation rate were observed on unmodified PEGDA hydrogels as a result of the extremely hydrophilic environment [17, 27]. When a scaffold is immersed into a physiological environment, the proteins in the ECM adsorb onto the scaffold within seconds, forming a protein layer which mediates the biological behaviour of seeded cells [28]. In this study, although the modified hydrogels were more hydrophilic than the unmodified hydrogel, it was found that the protein adsorption was significantly enhanced in a dose-dependent manner with the increasing concentrations of SMAS in the hydrogel. Because of the chemical and structural complexity of protein, the peptides along the adhesion-mediating protein backbone exhibited large and periodic charge alternations. For example, Fn Type III12–14, a domain function for both cell attachment and TGF- β 1 preservation, was continuous positively charged peptides in a physiological environment [15]. According to the results of the zeta potential assessment, the sulphamate incorporation could have led to a negatively charged hydrogel. Therefore, the sulphonated hydrogel could easily attract proteins by mutual electrostatic forces. Additionally, the strength of the electrostatic force depends on the charge density, which may explain why more proteins adsorbed onto the hydrogel with increasing concentration of SMAS. Furthermore, the chemistry of the sulphamate group is known to play an important role in affecting the orientation and conformation of adsorbed adhesion-mediating proteins, such as Fn, vitronectin, etc. For example, Felgueiras found that the sulphonated Ti6Al4V could promote the initial attachment and spreading of MC3T3-E1 cells by inducing the conformational alteration of Fn fibrillogenesis [29]. Pernodet found that, in the absence of cells, Fn can be converted from a soluble dimer

to an insoluble stable matrix on fibrous sulphonated polystyrene surfaces. It was demonstrated that Fn fibrillogenesis could result from the disulfide bond rearrangement caused by the catalysis of the sulphonated surface [30]. However, the effect of the sulphonated hydrogel on the conformational change in the ECM protein should be further studied.

The expression levels of ALP, osteogenic marker genes, and growth factors were evaluated to assess the effect of sulphonated hydrogels on osteoblastic differentiation [31]. ALP was proven to play an important role in the initiation of matrix mineralization [32, 33]. As shown in Fig. 8, compared with the HG0 group, the ALP activity of HG100 and HG200 groups was significantly enhanced at each time point, indicating the initiation of differentiation of a greater number of osteoblasts on the sulphonated hydrogel. However, the ALP activity was not significantly different between HG0 and HG50 groups, indicating that the improvement is associated with the concentration of SMAS in the hydrogel. Meanwhile, the gene expression level of osteogenic indicators, such as COL1 and OC, was evaluated. COL1 is the most abundant protein in bone ECM and binds to other non-collagenous matrix proteins [34, 35]. The up-regulated COL1 expression demonstrated that mature osteogenic ECM was formed and deposited on the sulphonated hydrogels. OC, the most specific marker of osteogenesis and mature osteoblasts, is present only in the bone matrix and is synthesized only by mature osteoblasts [27, 36, 37]. The enhanced expression levels of both early and late stage osteogenic indicators implies that the MC3T3-E1 cells on modified hydrogels proceeded through an accelerated differentiation mechanism, and matrix mineralization was activated by the sulphamate group [38, 39]. Meanwhile, the gene expression levels of well-established osteogenic growth factors, such as BMP-2 and TGF- β 1, were significantly up-regulated on the sulphonated hydrogels with increasing SMAS concentration. BMP-2 is a determinant factor in the development of the cell skeleton and regulates the anabolic and catabolic cycles of the osteoblast [40–43]. TGF- β 1 plays a critical role in modulating Runx2 transcriptional activity and matrix mineralization in the MC3T3-E1 cell line. Runx2 is a transcription factor involved in osteoblast differentiation and acts as an important regulator of bone formation at multiple stages [44, 45]. Correspondingly, in this study, the Runx2 expression levels of HG100 and HG200 groups were significantly up-regulated compared to that of the HG0 group at day 21. These results demonstrated that the sulphonated hydrogel could enhance osteoblastic differentiation, and the improvement is SMAS dose-dependent. However, determination of the underlying mechanism of improved osteoblastic differentiation on the sulphonated hydrogel requires further research.

5 Conclusions

To improve the biological performance of PEGDA hydrogel as a bone grafting scaffold, SMAS, a sulphonated monomer, was used to modify the PEGDA hydrogel. The results of FTIR and zeta potential analysis demonstrated that sulphonated hydrogels with different concentrations of sulphonate groups were fabricated. Based on the swelling ratio in deionized water and morphological observations, it was determined that a loose network was formed in the PEGDA-co-SMAS. The protein adsorption of PEGDA-co-SMAS was enhanced in accordance with increasing SMAS concentration. Meanwhile, in contrast to the pure PEGDA hydrogel, improved osteoblastic attachment, proliferation, and differentiation were found on the sulphonated hydrogel. The improvement level was associated with the concentration of SMAS. These results reveal that the sulphonated PEGDA hydrogel is a promising scaffold candidate for bone grafting. However, further research must be conducted to determine the precise mechanism underlying enhanced osteoblastic attachment, proliferation, and differentiation on modified hydrogels.

Acknowledgements This study was supported by Shandong Provincial Natural Science Foundation (ZR2018BH015).

Compliance with ethical standards

Conflict of interest The authors declare that they have no conflict of interest.

References

- Engberg K, Frank CW. Protein diffusion in photopolymerized poly(ethylene glycol) hydrogel networks. *Biomed Mater.* 2011;6:055006.
- Murphy SV, Atala A. 3D bioprinting of tissues and organs. *Nat Biotechnol.* 2014;32:773–85.
- Corbin EA, Millet LJ, Pikul JH, Johnson CL, Georgiadis JG, King WP, et al. Micromechanical properties of hydrogels measured with MEMS resonant sensors. *Biomed Micro.* 2013;15:311–9.
- Benoit DS, Schwartz MP, Durney AR, Anseth KS. Small functional groups for controlled differentiation of hydrogel-encapsulated human mesenchymal stem cells. *Nat Mater.* 2008;7:816–23.
- Schmidt S, Madaboosi N, Uhlig K, Kohler D, Skirtach A, Duschl C, et al. Control of cell adhesion by mechanical reinforcement of soft polyelectrolyte films with nanoparticles. *Langmuir.* 2012;28:7249–57.
- Sun K, Liu H, Wang S, Jiang L. Cytophilic/cytophobic design of nanomaterials at biointerfaces. *Small.* 2013;9:1444–8.
- Saxena S, Spears MW Jr., Yoshida H, Gaubling JC, Garcia AJ, Lyon LA. Microgel film dynamics modulate cell adhesion behavior. *Soft Matter.* 2014;10:1356–64.
- Pham MT, Reuther H, Maitz MF. Native extracellular matrix coating on Ti surfaces. *J Biomed Mater Res A.* 2003;66:310–6.
- Lehnert M, Gorbahn M, Rosin C, Klein M, Koper I, Al-Nawas B, et al. Adsorption and conformation behavior of biotinylated fibronectin on streptavidin-modified TiO(X) surfaces studied by SPR and AFM. *Langmuir.* 2011;27:7743–51.
- Felgueiras HP, Evans MD, Migonney V. Contribution of fibronectin and vitronectin to the adhesion and morphology of MC3T3-E1 osteoblastic cells to poly(NaSS) grafted Ti6Al4V. *Acta Biomater.* 2015;28:225–33.
- Tan F, Xu X, Deng T, Yin M, Zhang X, Wang J. Fabrication of positively charged poly(ethylene glycol)-diacrylate hydrogel as a bone tissue engineering scaffold. *Biomed Mater.* 2012;7:055009.
- Dadsetan M, Pumberger M, Casper ME, Shogren K, Giuliani M, Ruesink T, et al. The effects of fixed electrical charge on chondrocyte behavior. *Acta Biomater.* 2011;7:2080–90.
- Nakamura S, Kobayashi T, Nakamura M, Itoh S, Yamashita K. Electrostatic surface charge acceleration of bone ingrowth of porous hydroxyapatite/beta-tricalcium phosphate ceramics. *J Biomed Mater Res A.* 2010;92:267–75.
- Li H, Ji Q, Chen X, Sun Y, Xu Q, Deng P, et al. Accelerated bony defect healing based on chitosan thermosensitive hydrogel scaffolds embedded with chitosan nanoparticles for the delivery of BMP2 plasmid DNA. *J Biomed Mater Res A.* 2017;105:265–73.
- Pernodet N, Rafailovich M, Sokolov J, Xu D, Yang NL, McLeod K. Fibronectin fibrillogenesis on sulfonated polystyrene surfaces. *J Biomed Mater Res A.* 2003;64:684–92.
- Keselowky BG, Collard DM, Garcia AJ. Surface chemistry modulates fibronectin conformation and directs integrin binding and specificity to control cell adhesion. *J Biomed Mater Res A.* 2003;66:247–59.
- Hartvig RA, van de Weert M, Ostergaard J, Jorgensen L, Jensen H. Protein adsorption at charged surfaces: the role of electrostatic interactions and interfacial charge regulation. *Langmuir.* 2011;27:2634–43.
- Lou T, Wang X, Song G, Gu Z, Yang Z. Fabrication of PLLA/beta-TCP nanocomposite scaffolds with hierarchical porosity for bone tissue engineering. *Int J Biol Macromol.* 2014;69:464–70.
- Saha K, Pollock JF, Schaffer DV, Healy KE. Designing synthetic materials to control stem cell phenotype. *Curr Opin Chem Biol.* 2007;11:381–7.
- Cartmell SH, Thurstan S, Gittings JP, Griffiths S, Bowen CR, Turner IG. Polarization of porous hydroxyapatite scaffolds: influence on osteoblast cell proliferation and extracellular matrix production. *J Biomed Mater Res A.* 2014;102:1047–52.
- Anderson DG, Levenberg S, Langer R. Nanoliter-scale synthesis of arrayed biomaterials and application to human embryonic stem cells. *Nat Biotechnol.* 2004;22:863–6.
- Bacakova L, Filova E, Parizek M, Ruml T, Svorcik V. Modulation of cell adhesion, proliferation and differentiation on materials designed for body implants. *Biotechnol Adv.* 2011;29:739–67.
- Nuttelman CR, Benoit DS, Tripodi MC, Anseth KS. The effect of ethylene glycol methacrylate phosphate in PEG hydrogels on mineralization and viability of encapsulated hMSCs. *Biomaterials.* 2006;27:1377–86.
- Itoh S, Nakamura S, Kobayashi T, Shinomiya K, Yamashita K, Itoh S. Effect of electrical polarization of hydroxyapatite ceramics on new bone formation. *Calcif Tissue Int.* 2006;78:133–42.
- Wang X, Lou T, Zhao W, Song G, Li C, Cui G. The effect of fiber size and pore size on cell proliferation and infiltration in PLLA scaffolds on bone tissue engineering. *J Biomater Appl.* 2016;30:1545–51.
- Lou T, Wang X, Song G, Gu Z, Yang Z. Structure and properties of PLLA/beta-TCP nanocomposite scaffolds for bone tissue engineering. *J Mater Sci Mater Med.* 2015;26:5366.
- Olabisi RM, Lazard ZW, Franco CL, Hall MA, Kwon SK, Sevick-Muraca EM, et al. Hydrogel microsphere encapsulation of a cell-based gene therapy system increases cell survival of injected cells,

- transgene expression, and bone volume in a model of heterotopic ossification. *Tissue Eng Part A*. 2010;16:3727–36.
28. Hassan W, Dong Y, Wang W. Encapsulation and 3D culture of human adipose-derived stem cells in an in-situ crosslinked hybrid hydrogel composed of PEG-based hyperbranched copolymer and hyaluronic acid. *Stem Cell Res Ther*. 2013;4:32.
 29. Felgueiras HP, Decambron A, Manassero M, Tulasne L, Evans MD, Viateau V, Migonney V. Bone tissue response induced by bioactive polymer functionalized Ti6Al4V surfaces: in vitro and in vivo study. *J Colloid Interface Sci*. 2017;491:44–54.
 30. Tibbitt MW, Rodell CB, Burdick JA, Anseth KS. Progress in material design for biomedical applications. *Proc Natl Acad Sci USA*. 2015;112:14444–51.
 31. Rath B, Nam J, Knobloch TJ, Lannutti JJ, Agarwal S. Compressive forces induce osteogenic gene expression in calvarial osteoblasts. *J Biomech*. 2008;41:1095–103.
 32. Sharma B, Fermanian S, Gibson M, Unterman S, Herzka DA, Cascio B. et al. Human cartilage repair with a photoreactive adhesive-hydrogel composite. *Sci Transl Med*. 2013;5:167ra6
 33. Hao W, Jiang C, Jiang M, Wang T, Wang X. Osteogenic potency of dedifferentiated fat cells isolated from elderly people with osteoporosis. *Exp Ther Med*. 2017;14:43–50.
 34. Yang X, Yang K, Liao L, Jin Y. [Effect of miR-705 on osteogenic differentiation of mouse embryo osteoblast precursor cells MC3T3-E1]. *Zhejiang Da Xue Xue Bao Yi Xue Ban*. 2016;45:575–80.
 35. Marsh BC, Kerr NC, Isles N, Denhardt DT, Wynick D. Osteopontin expression and function within the dorsal root ganglion. *Neuroreport*. 2007;18:153–7.
 36. Wang D, Wang H, Gao F, Wang K, Dong F. CIC-3 promotes osteogenic differentiation in MC3T3-E1 cell after dynamic compression. *J Cell Biochem*. 2017;118:1606–13.
 37. Yao KL, Todescan R Jr., Sodek J. Temporal changes in matrix protein synthesis and mRNA expression during mineralized tissue formation by adult rat bone marrow cells in culture. *J Bone Miner Res*. 1994;9:231–40.
 38. Chen CH, Chang CH, Wang KC, Su CI, Liu HT, Yu CM. et al. Enhancement of rotator cuff tendon-bone healing with injectable periosteum progenitor cells-BMP-2 hydrogel in vivo. *Knee Surg Sports Traumatol Arthrosc*. 2011;19:1597–607.
 39. Canalis E, Economides AN, Gazzerro E. Bone morphogenetic proteins, their antagonists, and the skeleton. *Endocr Rev*. 2003;24:218–35.
 40. Shibata Y, Abiko Y, Moriya Y, Yoshida W, Takiguchi H. Effects of transforming growth factor-beta on collagen gene expression and collagen synthesis level in mineralizing cultures of osteoblast-like cell line, MC3T3-E1. *Int J Biochem*. 1993;25:239–45.
 41. Hughes FJ, Turner W, Belibasakis G, Martuscelli G. Effects of growth factors and cytokines on osteoblast differentiation. *Periodontol* 2000. 2006;41:48–72.
 42. Takahashi Y, Yamamoto M, Tabata Y. Enhanced osteoinduction by controlled release of bone morphogenetic protein-2 from biodegradable sponge composed of gelatin and beta-tricalcium phosphate. *Biomaterials*. 2005;26:4856–65.
 43. Chiang CW, Chen WC, Liu HW, Wang IC, Chen CH. Evaluating osteogenic potential of ligamentum flavum cells cultivated in photoresponsive hydrogel that incorporates bone morphogenetic protein-2 for spinal fusion. *Int J Mol Sci*. 2015;16:23318–36.
 44. Jeon EJ, Lee KY, Choi NS, Lee MH, Kim HN, Jin YH. et al. Bone morphogenetic protein-2 stimulates Runx2 acetylation. *J Biol Chem*. 2006;281:16502–11.
 45. Gersbach CA, Byers BA, Pavlath GK, Garcia AJ. Runx2/Cbfa1 stimulates transdifferentiation of primary skeletal myoblasts into a mineralizing osteoblastic phenotype. *Exp Cell Res*. 2004;300:406–17.